GPS Interference Detection and Identification Using Multicorrelator Receivers

Frédéric BASTIDE, *ENAC*
Eric CHATRE, *STNA*
Christophe MACABIAU, *ENAC*

BIOGRAPHY

Frederic Bastide graduated in July 2001 as an electronics engineer from the Ecole Nationale de l'Aviation Civile (ENAC) in Toulouse, France. He intends to become a researcher in satellite radionavigation.

Eric Chatre graduated as an electronics engineer in 1992 from the ENAC (Ecole Nationale de l'Aviation Civile), Toulouse, France. Since 1994, he has been working with the Service Technique de la Navigation Aérienne (STNA) in Toulouse on implementation of satellite navigation in civil aviation. He is involved in the development of EGNOS and in the definition phase of Galileo. He is also participating in GNSS standardization activities in ICAO GNSSP and EUROCAE, RTCA forums.

Christophe Macabiau graduated as an electronics engineer in 1992 from the ENAC (Ecole Nationale de l'Aviation Civile) in Toulouse, France. Since 1994, he has been working on the application of satellite navigation techniques to civil aviation. He received his Ph.D. in 1997 and has been in charge of the signal processing lab of the ENAC since 2000.

ABSTRACT

The interference is among the most feared events in civil aviation use of GNSS. A large number of techniques were designed to alleviate the sensitivity of modern receivers to this perturbation. Most of these techniques are either based on spatial discrimination like adaptive antennas, on spectral selectivity such as notch filters or on amplitude detection. The advent of multicorrelator receivers widens the range of post-correlation methods that can be considered to tackle this problem. In particular, this enables the characterization of interference effects on the tracking loops through the analysis of the shape of the correlation peak.

The aim of this paper is to present the technique we have developed to detect and identify the interference parameters using a multicorrelator receiver and to detail the results obtained during testing with CW and FM jammers.

The paper starts with the theoretical derivation of the effect of CW interference on the code and phase tracking loops I and Q samples for a typical receiver. Results of CW interference tests are described for different test configurations.

Correlation peaks are collected for different CW interferer frequencies and power levels. These observations were used to validate the theoretical derivations mentioned above, therefore demonstrating the feasibility of interference detection with multicorrelator techniques. These tests were further extended to FM type interference with different bandwidths and power levels and yielded similar results.

The paper goes on describing the processing steps implemented to estimate interference characteristics (central frequency, bandwidth and power) using different parametric methods (Prony Covariance, truncated SVD and ESPRIT).

Performance of these techniques is then assessed on data collected using a multicorrelator receiver connected to a GPS signal RF generator and affected by several CW and FM interferers with different power levels, bandwidth and central frequency.

Finally, a real time tool allowing interference detection and estimation is presented.

I. INTRODUCTION

Several types of perturbations can affect the signal processed by a GPS receiver. These perturbations are thermal noise, atmospheric disturbances, multipath and interference. Interference remains the most feared perturbation for civil aviation users because it can affect several tracking channels at a time during a long period.

This is a serious problem since it can first affect the continuity of the navigation service and necessitate reversal to other means of navigation or assistance from the air traffic services. Different techniques have been presented to improve robustness of receivers against interference [Spilker and Natali, 1996] based on antenna, RF front end and/or signal processing module designs [Przyjemski et al., 1993]. However, if interference is not

mitigated by implemented techniques, it can also affect the integrity of the pseudorange measurements. In particular, RAIM algorithms implemented in all aviation receivers to ensure integrity are designed to meet their requirements only when there is a unique failure. The case of interference is therefore not obviously protected by RAIM techniques.

For this reason, there is a need to develop a module able to detect and characterize jammers affecting the receiver processing. Such a module would be most helpful if imbedded in the receiver and not requiring any heavy external equipment such as spectrum analyzer.

The following paper discusses the use of multicorrelator receivers to achieve such a goal.

II. EFFECT OF CW TONE ON I AND Q SAMPLES

The effect of a CW type interference was studied and presented earlier in details by the authors. In particular, the output of the Integrate and Dump Filters for the I and Q channels has been shown in [Macabiau, Julien, Chatre, 2001] to be:

$$\begin{cases} I(n) = \dfrac{A}{2} D(n) R(\varepsilon_D) \cos \varepsilon_P \\ + \dfrac{A_J}{2} T_D \left| C_{\text{sinc}}(k_0) \right| \dfrac{\sin \pi \delta f T_D}{\pi \delta f T_D} \cos\left(2\pi k_0 f_R \hat{\tau} + \varphi(n)\right) \\ + n_I(n) \\ Q(n) = \dfrac{A}{2} D(n) R(\varepsilon_D) \sin \varepsilon_P \\ - \dfrac{A_J}{2} T_D \left| C_{\text{sinc}}(k_0) \right| \dfrac{\sin \pi \delta f T_D}{\pi \delta f T_D} \sin\left(2\pi k_0 f_R \hat{\tau} + \varphi(n)\right) \\ + n_Q(n) \end{cases}$$

where

- A is the amplitude of the line-of-sight signal
- D and C are the P/NRZ/L waveforms associated to the navigation message and to the C/A code
- θ is the carrier phase shift of the line-of-sight signal
- τ is the group propagation delay of the line-of-sight signal
- A_J is the amplitude of the CW jammer
- Δf is the frequency offset of the transmitted jammer signal with respect to L1
- θ_J is the time-dependent phase shift of the jammer
- n is the index of the time series at the output of the I&D filters.
- $\varepsilon_P = \theta - \hat{\theta}$ is the carrier phase tracking error.
- $\varepsilon_D = \tau - \hat{\tau}$ is the code tracking error.
- T_D=20 ms is the I&D integration duration and $f_D = 1/T_D$.
- f_R=1 kHz is the C/A code repetition frequency.
- k_0 is the index of the C/A code spectrum line such that $k_0 f_R \in \left[\Delta f - \dfrac{f_D}{2}; \Delta f + \dfrac{f_D}{2} \right]$.
- $\Delta\theta = \theta_J - \hat{\theta}$ is the phase difference between the jammer and the local carrier.
- $\varphi(n) = 2\pi\left(\Delta f - k_0 f_R\right)\dfrac{T_n}{2} - \Delta\theta + \varphi(k_0)$ and $T_n = (n - 0.5)MT_s$ is the centre of the current summation window (M is the number of samples accumulated by the I&D filters).
- $\delta f = k_0 f_R - \Delta f$
- n_I and n_Q are the signals resulting from the integration of the noise samples.

The two additional terms in the I and Q samples delivered by the I&D filters are in fact the result of the correlation between the local generated code and the additive CW tone.

The result of that correlation is easier to understand in the frequency domain because a correlation operation between two signals can be viewed as the product of the Fourier transforms of the first signal with the conjugate of the Fourier transform of the second signal.

The Fourier transform of the windowed jammer is composed of two *sinc* with a main lobe of width *[-50 Hz; +50 Hz]* located in -Δf and +Δf, as illustrated in figure 1.

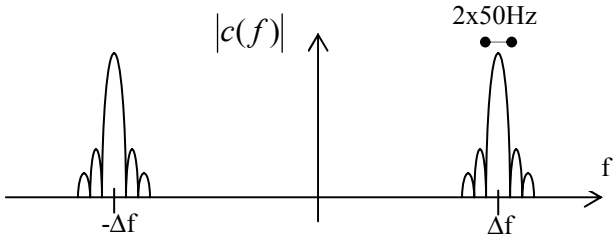

Figure 1: *Magnitude of Fourier transform of windowed CW jammer*

Similarly, the discrete signal Fourier transform of C is the product of the Fourier transform of the P/NRZ/L waveform with the Fourier transform of the C/A Gold code. This discrete signal Fourier transform can be expressed as:

$$C_d(f) = \sum_{k=-\infty}^{+\infty} \frac{1}{1023} \frac{\sin \dfrac{\pi k}{1023}}{\dfrac{\pi k}{1023}} C_0(k) \delta\left(f - k f_R\right)$$

for $f \in \left[-\dfrac{F_s}{2}; \dfrac{F_s}{2} \right[$, where C_0 is the discrete Fourier transform of the tracked C/A Gold code. This discrete Fourier transform C_0 is periodic with period 1023.

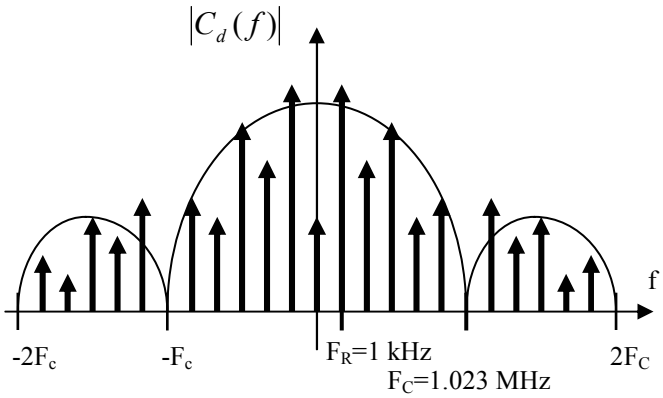

Figure 2: *Magnitude of Fourier transform of P/NRZ/L waveform representing the C/A code.*

As illustrated in figure 2, $C_d(f)$ is a pure line spectrum. Each dirac line has a weight which is the product of the *sinc* weighting function originating from the P/NRZ/L materialization of the code, with the individual weight of the line in the C/A code discrete Fourier transform.

We can simplify this expression into

$$C_d(f) = \sum_{k=-\infty}^{+\infty} C_{\text{sinc}}(k)\delta\left(f - kf_R\right)$$

where $C_{\text{sinc}}(k) = \frac{1}{1023}\frac{\sin\frac{\pi k}{1023}}{\frac{\pi k}{1023}}C_0(k)$.

where k_0 is the index of the C/A code spectrum line such that $k_0 f_R \in \left[\Delta f - \frac{f_D}{2}; \Delta f + \frac{f_D}{2}\right]$.

Therefore, as we can see from these final expressions, the I and Q correlator outputs of the tracking loops are disturbed by additive cosine and sine terms. The influence of the jammer highly depends on the relative amplitude of these additive oscillations with respect to the amplitude of the received line-of-sight code correlation. This relative amplitude depends

- on the direct ratio of the received jammer power with respect to the received GPS signal power
- on the 50 Hz *sinc* of the frequency offset of the received jammer with respect to the received signal frequency
- on the weight of the P/NRZ/L C/A code line which is being hit by the jammer

III. MULTICORRELATOR RECEIVERS

To detect the presence of interfering signals in the tracking loops, we have decided to use a Novatel Millenium multicorrelator receiver. To test the performance of the detection and estimation technique, we also conducted some experiments with an interference generator, a RF GPS signal generator and the receiver.

Classical receivers offer several tracking channels, each of them being driven by two pairs of correlator outputs. A multicorrelator receiver provides values of the correlation of the incoming signal with several delayed replicas of the same local code in a single tracking channel. In that case, we get simultaneously several I and Q samples for each relative delay *d* of each replica with respect to punctual.

For the experiment described here, we have used a Novatel Millenium receiver whose software has been modified so as to provide 2 tracking channels, one of them just providing 2 correlator outputs on I and Q, and the second one providing 46 correlator outputs both on I and Q for interference analysis. The desired offset of the 46 correlators with respect to punctual was designed by setting a compromise between the resolution and the maximum interfering signal frequency that can be identified. We have decided to place the 46 correlators with a step of 0.25 chip from –5.9 chips to 5.1 chips from punctual. This provides an analysis window of 11 chips, and enables an unambiguous detection of interfering signals up to 2 MHz around L1.

The operations performed in each correlation channel are illustrated in figure 3.

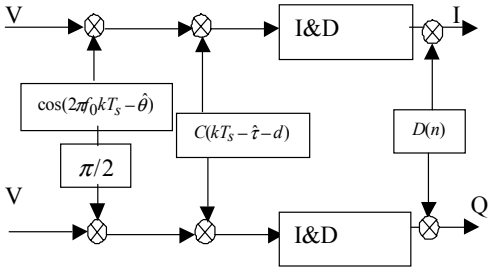

Figure 3: *Architecture of one correlator output.*

We can deduce the expression of the correlator outputs in presence of a CW jammer from the final expressions obtained in section II.

$$\begin{cases} I(n) = \frac{A}{2}R(\varepsilon_D - d)\cos\varepsilon_P \\ + \frac{A_J}{2}T_D D(n)\left|C_{\text{sinc}}(k_0)\right|\frac{\sin\pi\delta f T_D}{\pi\delta f T_D}\cos\left(2\pi k_0 f_R d + \psi(n)\right) \\ + n_I(n) \\ Q(n) = \frac{A}{2}R(\varepsilon_D - d)\sin\varepsilon_P \\ - \frac{A_J}{2}T_D D(n)\left|C_{\text{sinc}}(k_0)\right|\frac{\sin\pi\delta f T_D}{\pi\delta f T_D}\sin\left(2\pi k_0 f_R d + \psi(n)\right) \\ + n_Q(n) \end{cases}$$

where $\psi(n) = 2\pi k_0 f_R \hat{\tau} - \varphi(n)$.

The interference generator is a Rohde and Schwarz signal generator SME03. It is used in this experiment to generate a CW tone and an FM modulated carrier. The uncertainty in the output power level was determined to be ± 1 dB W for power levels around –100 dB W.

IV. IMPACT OF INTERFERENCE

The practical analysis of the impact of interference on correlator outputs is presented in detail in [CHATRE et al., 2001]. In this paper, we just recall the main characteristics of that effect that are used by the interference detection and estimation technique.

The effect of CW interference has been illustrated on PRN 6. The highest line of PRN 6 C/A code has a frequency of 227 kHz and an individual relative power of –21.29 dBW with respect to the total power of the C/A code.

To jam that code line, we configured the GPS signal generator with a scenario in which the Doppler of the received PRN 6 signal crosses 0. The CW signal generator was set to deliver a tone at L1+227 kHz with an output power of -132 dBW. Considering the 3dB coupler used to add the GPS signals and the jammer, the power of the interferer at the input of the receiver is therefore –135 dBW, and the power of the GPS signal is –143 dBW.

Figure 4 shows the evolution of the C/N_0 as computed by the receiver throughout the test. As we can see, in the beginning of the test, when no jammer is present, the C/N0 is equal to 49 dB Hz.

Throughout the experiment, the tracking channel never experienced loss of lock. During the first minute after the jammer is turned on, the estimated C/N_0 oscillates between 45.5 dB Hz and 49.5 dB Hz. After this transient period, the C/N_0 estimate is stable at 48.4 dB Hz, which is 0.6 dB below its initial value.

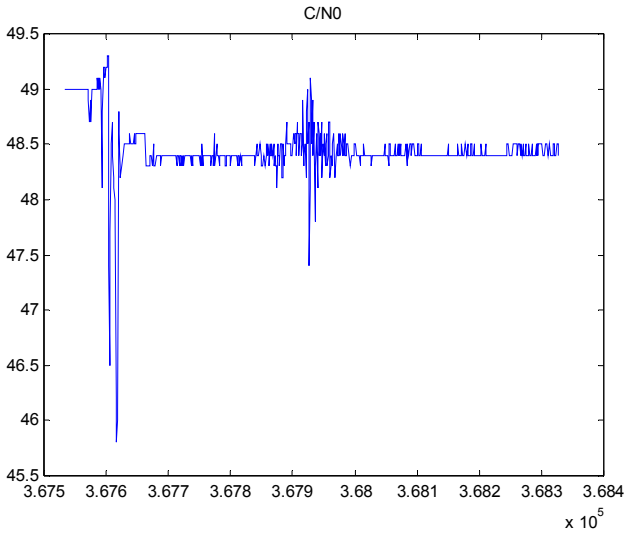

Figure 4: *Evolution of the C/N_0 as estimated by the receiver.*

As we can see on this graph, 250 seconds after the jammer has been powered on, the estimated C/N_0 starts to oscillate, its time evolution being constrained in a *sinc* envelope. That effect is clearly the illustration of the evolution of the correlation between the CW tone and the C/A code. Indeed, during the first 250 s, the cross-correlation is 0 because the jammer does not interact with any C/A code line. Then, as the received signal doppler shift nears 0, the correlator output is increasingly affected by the sine function resulting from the cross-correlation between the jammer and the targeted C/A code line.

The shape of the envelope of this sine function is determined by the *sinc* appearing in the expressions presented in section II. The argument of this *sinc* function is the frequency offset δf between the jammer and the targeted C/A code line, which is driven by the quasi-linear evolution of the doppler in this time interval.

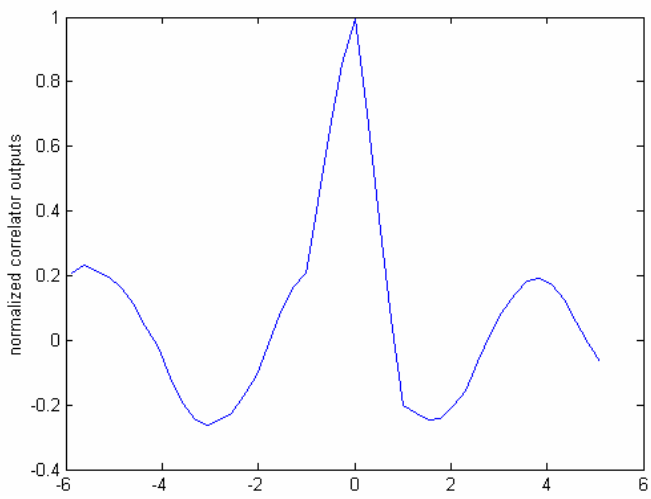

Figure 5: *Observed correlation function.*

As an example, figure 5 shows the output correlation function at the epoch where the amplitude of the sine function is maximum. We can clearly see that this function is the sum of the nominal triangle and the sine function. In this figure, the period of this sine function is 4.5 chips which corresponds to a frequency of 227 kHz.

Another type of tests that were conducted aimed at analyzing the effect of larger band interference. The interference generator was then configured to generate a frequency modulated carrier. The modulation signal is simply a sine function. The carrier is set to be at L1+227 kHz.

For the first series of tests presented here, the single-sided bandwidth of the spectrum is 50 kHz. The total power of the FM signal is -110 dB W.

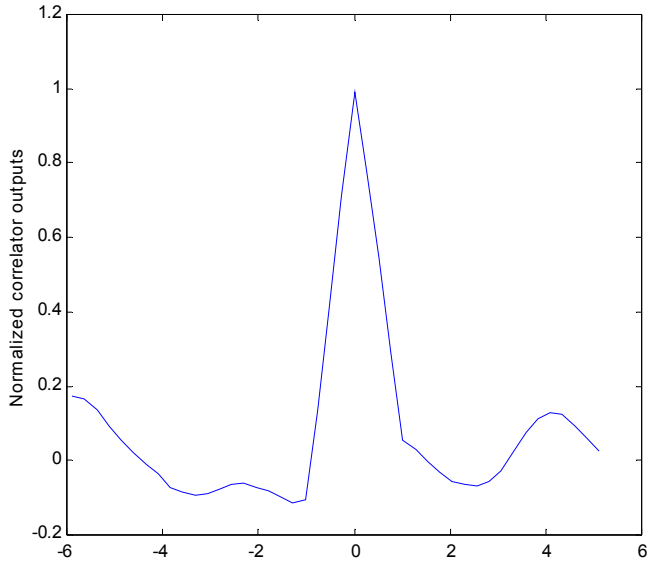

Figure 6: *Correlator output showing the result of the correlation between the 50 kHz FM signal and the C/A code.*

As an example, figure 6 shows the output correlation function at one particular epoch. As it appears in this figure, this function is dominated by the 227 kHz tone plus other oscillations. This function can be interpreted from the results presented in section II as the sum the cross-correlation between the sine functions composing the FM signal and the 100 targeted C/A code. As the amplitude of these correlation functions is determined by the power level of the C/A code hit line, the most powerful resulting function is the 227 kHz tone.

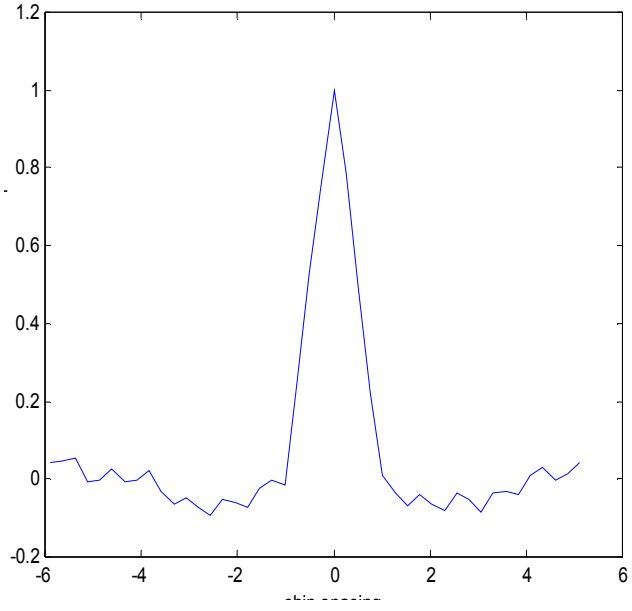

Figure 7: *Correlator output showing the result of the correlation between the 200 kH FM signal and the C/A code.*

As an example, figure 7 shows the output correlation function at one particular epoch. As it appears in this figure, this function is affected by several oscillations and the 227 kHz tone is no longer the dominant result, as 400 C/A code lines are impacted.

V. OVERVIEW OF PROPOSED TECHNIQUE

The theoretical and practical analyses presented in sections II and IV show that the correlator outputs of a GPS receiver are affected by an additional sinusoidal term whose amplitude and frequency are dependent upon the jammer characteristics.

Therefore, we decided to test for the presence of a sine function to decide whether the receiver is affected by a jammer, and to determine its characteristics to estimate the jammer signature (central frequency, bandwidth).

The first step is then to detect the presence of a disturbing interference, which is an interference signal that distorts the correlator outputs. That is done by computing the FFT of the correlator outputs at each epoch and comparing the maximum value of the FFT magnitude to a preset threshold.

In case of a positive detection, the second step is to remove the line-of-sight correlation peak from the correlator outputs. That is done in two stages: first of all, the correlator outputs are normalized with respect to the total power at the output of the punctual correlators. Then, the average value of the correlation function is subtracted from that normalized output.

The corner stone of the process is to run a specialized procedure on the residuals to determine the number of sine functions present and their respective frequency. This uses parametric methods based on AR-models such as Prony or ESPRIT.

Finally, the successive instantaneous estimates are post-processed statistically in order to improve the performance of the overall tool.

VI. PARAMETRIC METHODS

Parametric spectrum analysis techniques are suited for our application because they offer superior frequency resolution. The most adapted models for our situation are the AutoRegressive (AR) models and the Prony models. Two High Resolution techniques, that have the capacity to detect sinewaves with extremely close frequencies are also considered: the truncated SVD and the ESPRIT algorithm. Of course, other parametric models do exist, but they have not been considered as it was anticipated that they would offer a lower performance in our application [Castanié, Mailhes, Ducasse, 1997].

Complete theory on these techniques is available in many material, only the main developments are recalled.

AR MODELS

The ARMA model assumes that the sampled stochastic signal $x(n)$ can be modeled as the output of a digital filter F(z) excited by a zero-mean white noise $e(n)$:

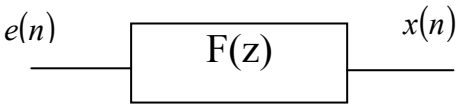

where

$$F(z) = \frac{\sum_{k=0}^{q} b_k Z^{-k}}{\sum_{k=0}^{p} a_k Z^{-k}}$$

and $E[e(n)] = 0$, $E[e(n)e^*(n-k)] = \sigma_e{}^2 \delta_k$, $\sigma_e{}^2$ being the power of the white noise.

Therefore $x(n)$ can be expressed as a ARMA(p,q) model:

$$x(n) = -\sum_{k=1}^{p} a_k x(n-k) + \sum_{k=0}^{q} b_k e(n-k)$$

The objective of the parameter model identification technique is to determine the p+q+1 a_k and b_k parameters and the input noise power $\sigma_e{}^2$.

An AR model can be expressed as $x(n) = -\sum_{k=1}^{p} a_k x(n-k) + e(n)$ with the filter $F(z) = \frac{1}{1 + \sum_{k=1}^{p} a_k Z^{-k}}$

An estimate of the modeled signal is:

$$\hat{x}(n) = -\sum_{k=1}^{p} a_k x(n-k)$$

therefore $e(n)$ can be expressed as:

$$e(n) = x(n) - \hat{x}(n)$$

and is called the linear prediction error or power residual $\sigma_e{}^2$.

The popular Yule-Walker technique can be used to determine the a_k such that they minimize the following squared prediction error criterion:

$$E = \sum_{n=1}^{N} |e(n)|^2 = \sum_{n=1}^{N} \left| \sum_{k=0}^{p} a_k x(n-k) \right|^2$$

Other methods are available to compute the a_k parameters. They differ by the error criterion they minimize. The covariance technique is the technique we will use in our application.

The covariance technique consists in minimizing the estimated power of the linear prediction error defined as:

$$\hat{E} = \frac{1}{N-p} \sum_{n=p}^{N-1} \left| x(n) + \sum_{k=1}^{p} a_k x(n-k) \right|^2$$

We could also have used the correlations technique, however [Lambert-Nebout, 1989] indicates that the covariance technique is the best adapted for the determination of the frequency content in a signal when very few samples are available.

The truncated SVD technique is a high resolution technique that uses the existence of a signal sub-space and a noise sub-space to determine the a_k. In the absence of noise, the covariance matrix of a signal composed of n pure sinewaves has a rank $2n$. The presence of noise increases the rank. The principle of the truncated SVD technique consists in forcing the rank of the covariance matrix to $2n$. To do that, the lowest sigular values, corresponding to noise, are set to 0 while the $2n$ largest singular values, modelling the useful signal, are not modified.
The application of that method requires the exact knowledge of the number of sinewaves in the signal

In presence of $2n$ sinewaves, the minimal theoretical order of an AR model is $2n$
In practice, the order p must be selected larger than the theoretical order in order to take the noise into account and to limit its effects. The order will be selected such that $p > 2n$.
However, the order selected must not be too high in the other case peuvent venir perturber l'analyse spectrale..

The two most popular estimators of the number of sinewaves contained in a signal are the *AIC criterion* (Akaike Information Criterion) and the *MDL criterion* (Minimum Description Length) that can be expressed as a function of the eigen values of the autocorrelation matrix [Castanié,Mailhes,Ducasse, 1997]. These criteria reflect the power of the error of the AR model for each of the order k up to the order $p-1$.

The order for which these criteria are minimum correspond to the order of the AR model. This number

must be divided by two to determine the number of sinewaves.

PRONY MODELS

The Prony model assumes the discrete signal x(n) is a sum of complex exponential expressed as:

$$x(n) = \sum_{k=1}^{p} b_k Z_k^n + e(n)$$

where

- $b_k = A_k \exp(j\theta_k)$, A_k is the amplitude of the k mode and θ_k is the phase in radians
- $Z_k = \exp((\alpha_k + j2\pi f_k)T)$, α_k is the damping factor and f_k is the frequency in Hertz. T is the sampling frequency

p is the model order and $e(n)$ is the model error.

The error criterion we have selected is the one used by the extended Prony method

$$\frac{1}{N-p}\sum_{n=p}^{N-1}\left|x(n)+\sum_{k=1}^{p}a_k x(n-k)\right|^2 = \frac{1}{N-p}\sum_{n=p}^{N-1}E^2(n)$$

The resolution is achieved in three steps :

- determination of the a_k
- determination of the Z_k. At this stage, the frequencies and associated damping factors can be estimated:

$$\alpha_k = \frac{Ln|Z_k|}{T} \quad \text{and}$$

$$f_k = Arctg\left(\frac{\mathrm{Im}(Z_k)}{Re(Z_k)}\right)/2\pi T$$

- determination of the b_k The amplitudes and phases of the different modes are then obtained directly:

$$A_k = |b_k| \qquad \text{and} \qquad \theta_k = Arctg\left(\frac{\mathrm{Im}(b_k)}{Re(b_k)}\right)$$

If the number n of sinewaves in the signal is known, the $2n$ (n in the complex case) corresponding poles are the less damped ones or those that are closer to the unit circle.

Once the poles of the signal are identified, it is easy to determine the amplitudes and the corresponding phases.

An estimation of the poles of the signal can also be obtained using the high resolution ESPRIT algorithm (Estimation of Signal Parameters via Rotational Invariance Techniques) that uses the property of rotation of the signal sub-space.

These methods were applied on different input signals I correlator outputs only, Q only and I+iQ.

VII. TESTS RESULTS

In the first test presented, the GPS signal of PRN 6 is affected by a single CW interference with the following characteristics : Power –100 dBm at the output of the generator (3dB coupler is used – see section IV), Center frequency L1+227 kHz. The initial doppler of PRN 6 is about 400 Hz with a doppler rate of about -0.5 Hz/s. This means that the 227th line of the CA code will slowly cross the jammer CW during the scenario.

Figure 8 shows the value of the detection flag as a function of time into the scenario. One can clearly see that detections appear about 200s after the beginning which corresponds to the time when the 227th CA code line crosses the second side lobe of the windowed jammer. This ensures an early warning before the worst of the interference hits the signal processing. Afterwards, the number of detections is maximum accross the main lobe. This is were most of the characterisation of interference will take place.

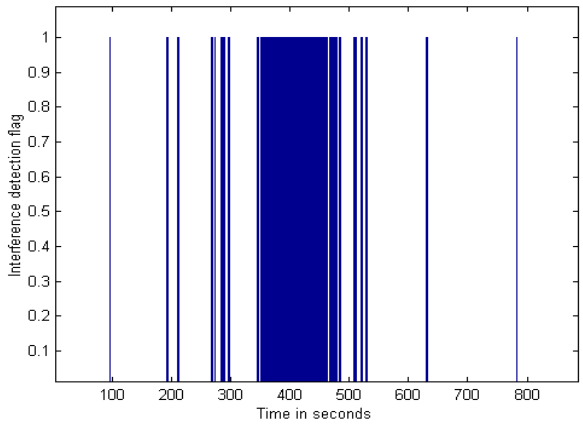

Figure 8: Interference Detection Flag as a function of time for CW jammer scenario

Figure 9 shows the estimate of amplitude of the sine wave given by the Prony model as a function of time. Again, the characteristic shape of the windowed jammer (sinc^2) is easily recognizable.

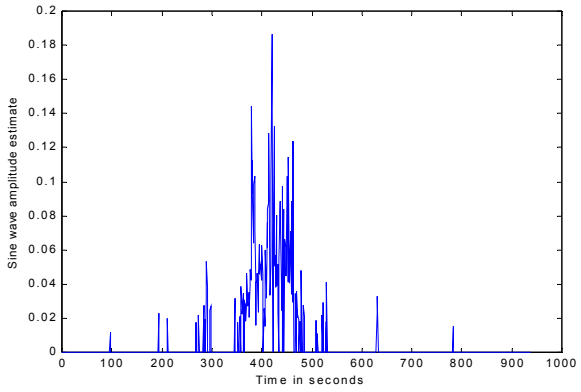

Figure 9 : Estimate of amplitude of sine as a function of time for CW jammer scenario using Prony Covariance.

Figure 10 presents the order of the AR-model estimated by the MDL algorithm throughout the scenario. Except for one sample, the order estimate is consistently equal to 2. This signifies that the algorithm forecasts the presence of a single sinewave in the signal processed. It is therefore consistent with the CW test. Similar results were obtained using the AIC algorithm.

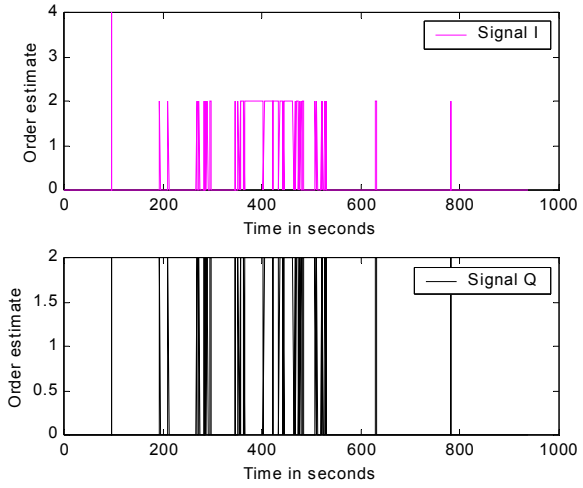

Figure 10 : Order of AR-model estimated using MDL algorithm for CW jammer scenario

Once the detection flag is raised and the MDL algorithm has predicted the number of sine waves in the signal, the estimation model is launched using one of the three methods described in section VI. Figure 11 shows the histograms of frequency estimates provided by the Prony Covariance algorithm for different input signals. The scenario considered is still a CW jammer but the AR-model is launched on I samples only, Q samples only and finally the composite complex signal I+iQ. Results show that the estimation process yields good performance and allows a good characterisation of the jammer center frequency. The standard deviation of the estimate is slightly better for the I+iQ case and slightly degraded for the Q only case but remains in all cases less than 10 kHz.

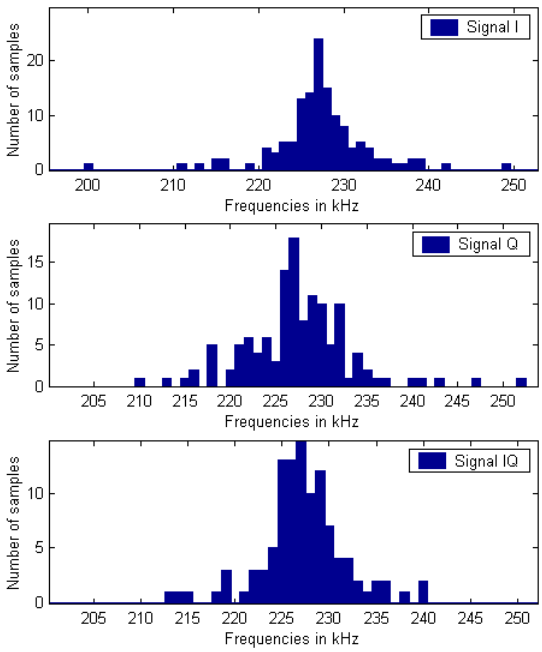

Figure 11 : Histograms of frequency estimates using Prony Covariance method.

The final step in the overall characterization process is to use successive estimates to improve performance. The statistical post-processing based on cluster analysis removes outliers and filters data over a sliding window. Figure 12 shows the final output of the estimation tool. One can see that, over the whole scenario, the center frequency estimate is very close to the real value (L1+227 kHz) regardless of the input signal used (I, Q or I+iQ). The standard deviations obtained are close to 1 kHz. This is a significant improvement over the raw output of the instantaneous Prony model.

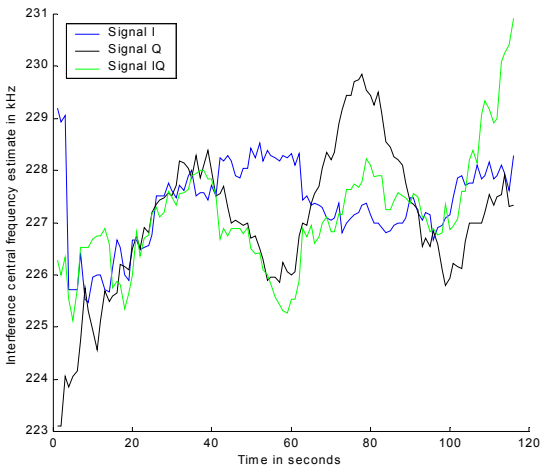

Figure 12 : Estimates of jammer central frequency after statistical post-processing.

It is to be noted that the setting of estimation thresholds used to trig the Prony model has a strong influence on the performance of the process. Indeed, the higher the

threshold is set, the better is the end results since only signals with strong and clear sinewaves are passed to the parametric models.

Finally, the tool was also tested on wide band interference simulated using a FM modulation. Figures 13 and 14 present estimates of center frequency and bandwidth for a scenario with an FM jammer at L1+265 kHz with a bandwith varying from 100kHz to 200kHz. The jammer power is - 80dBm at the output of the generator.

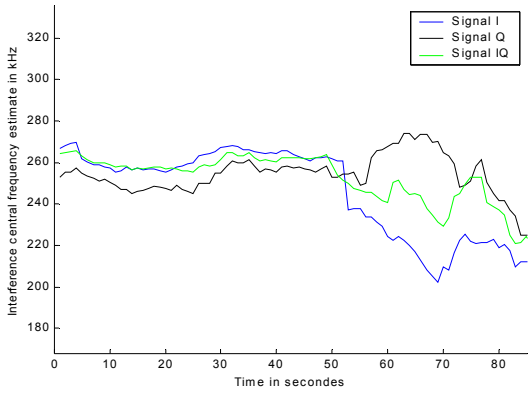

Figure 13 : Estimate of center frequency for FM type modulation

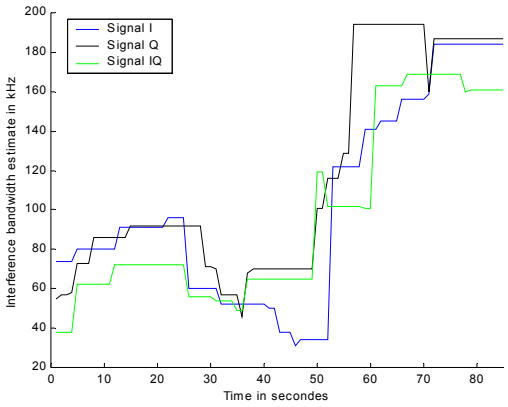

Figure 14 : Estimate of bandwidth for FM type modulation

Once again the results show that the tool performs very well and provides reliable characterization of the interference parameters.

Finally, Figure 15 presents the MMI of the final product called InSPECT (Interference Sensing by Parametric Estimation and Calibration Techniques). The different graphs display the input signals to be modelled, the results of the instantaneous estimation process as well as the output of the post-processing. The number and type of interference detected are also presented to the user along with an estimate of the aggregate jammer power based on the value of the AGC gain after calibration in laboratory.

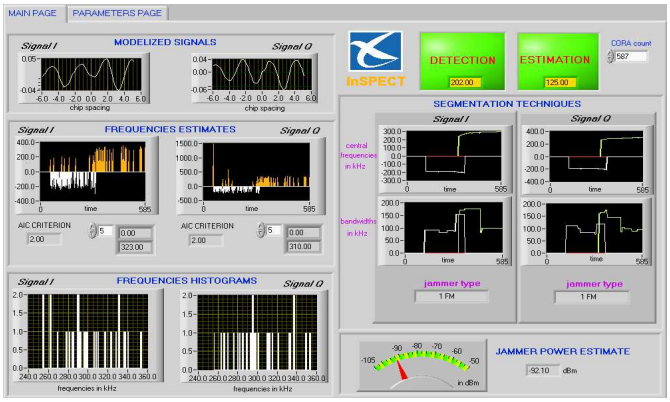

VIII. CONCLUSION

The theoretical developments presented in the second section show the impact of a CW jammer on the correlator outputs. The predicted amplitude of the induced perturbation depends on the relative amplitude of the jammer and the received GPS signal, on the frequency offset between the jammer and the nearest C/A code line and on the weight of that spectrum line.

Observations of the correlator outputs using a multicorrelator receiver confirmed these results in several test cases involving CW jamming at different frequencies and power levels. Additional tests showed that the CW analysis could be extended by a superposition principle to cover Wide Band jammers that affect simultaneously a number of CA code lines.

The study showed that detection of interference can be triggered reliably based on computation of FFT of the raw correlator outputs and that AR-modeling was able to provide accurate estimates of interference characteristics such as center frequency or bandwidth. Several AR-models were tested giving satisfactory results with a slight advantage to the Prony Covariance methods that yielded less dispersion in the results. The best results were also obtained when both I and Q channels were processed simultaneously in a composite complex signal I+iQ.

Finally, filtering and post-processing of raw estimates showed significant improvements in the performance of the overall estimation process. This statistical processing brought robustness with regards to outliers and additional stability to the final results.

The real time tool developed during this study and integrating all processing steps described above provides an efficient, cheap and reliable way to detect and characterize quickly interference affecting a GNSS receiver.

REFERENCES

[Castanié, Mailhes, Ducasse, 1997], F. CASTANIE, C. MAILHES and A. DUCASSE, “Estimation de fréquences:

Panorama des méthodes paramétriques", ENSEEIHT-GAPSE

[Lambert-Nebout, 1989], C. LAMBERT-NEBOUT, "Etude des moyens d'analyse du signal basse fréquence d'un récepteur d'alignement de piste ", Ph.D. Thesis INPT.

[Macabiau, Julien, Chatre, 2001], C. MACABIAU, O. JULIEN and E. CHATRE, "Use of Multicorrelator Techniques for Interference Detection", proceedings of ION NTM 2001.

[Przyjemski et al., 1993], J. PRZYJEMSKI, J. BALBONI, E. DOWDLE and B. HOLSAPPLE, "GPS Anti-Jam Techniques", proceeding of ION GPS-93

[Spilker and Natali, 1996], J. SPILKER and F. NATALI, "Interference Effects and Mitigation Techniques", Chapter 20 of 'Global Positioning System: Theory and Applications', AIAA.